Inhibition of polymorphic MexXY-OprM efflux system in Pseudomonas aeruginosa clinical isolates by Berberine derivatives

WILEY VCH

RESEARCH ARTICLE

Inhibition of polymorphic MexXY-OprM efflux system in *Pseudomonas aeruginosa* clinical isolates by Berberine derivatives

Giorgia Giorgini [a], Alessandra Di Gregorio[a], Gianmarco Mangiaterra[b], Nicholas Cedraro[a], Cristina Minnelli[a], Giulia Sabbatini[a], Giovanna Mobbili[a], Serena Simoni[a], Carla Vignaroli[a], Roberta Galeazzi[a]*

[a] Dr. G., Giorgini, A., Di Gregorio, Dr., N., Cedraro, Dr. G. Minnelli, G. ,Sabbatini, Dr. C., Minnelli, Prof. G., Mobbili, Dr. S., Simoni, Prof. C., Vignaroli, Prof. R., Galeazzi
Department of Life and Environmental Sciences
Polytechnic University of Marche
via Brecce Bianche, 60131, Ancona, Italy
E-mail: r.galeazzi@univpm.it

[b] Dr. G., Mangiaterra
Department of Biomolecular Sciences, University of Urbino Carlo Bo, 61029 Urbino, Italy;

Supporting information for this article is given via a link at the end of the document.

Abstract: The MexXY-OprM multidrug efflux pump (EP) in aminoglycosides resistant *Pseudomonas aeruginosa* is one of the major resistance mechanisms, which is often overexpressed in strains isolated from pulmonary chronic disease such as cystic fibrosis [1–3]. In this research, we focused on the design of potential efflux pumps inhibitors, targeting MexY, the inner membrane component, in an allosteric site. Berberine [4] has been considered as lead molecule since we previously demonstrated its effectiveness in targeting MexY in laboratory reference strains [5,6]. Since this protein is often present in polymorphic variants in clinical strains, we sequenced and modeled all the mutated forms and we synthesized and evaluated by computational techniques, some berberine derivatives carrying an aromatic functionalization in its 13-ring position. These compounds were tested *in vitro* against clinical *P. aeruginosa* strains for antimicrobial and antibiofilm activity. In conclusion, The results demonstrated the importance of the aromatic moiety functionalization in exerting the EP inhibitory activity in synergy with the aminoglycoside tobramycin. More, we found that aminoacidic composition of MexY in different strains must be considered for predicting potential binding site and affects the different activity of berberine derivatives. Finally, the antibiofilm effect of these new EPIs is promising, in particular for o-CH3-berberine derivative.

Introduction

The multidrug efflux system MexXY-OprM, within the resistance-nodulation-division family (RND), is the major efflux pump (EP) involved in the aminoglycoside resistance in *Pseudomonas aeruginosa* [1,7,8]. At present, the high incidence of multi-drug-resistant (MDR) *P. aeruginosa* strains overexpressing the MexXY-OprM pump in cystic fibrosis (CF) pulmonary infections have been underlined. The MexXY-OprM is a tripartite efflux pump including a periplasmic membrane fusion protein (MexX), the inner membrane (IM) drug/H^+ antiporter (MexY; the RND component), and the outer-membrane (OM) channel (OprM). Crystal structures of this EP is still lacking but other *P. aeruginosa* efflux pump proteins such as MexB [9], as well as the related AcrB of *Escherichia coli* [10] are instead resolved. Based on these reported data, the 3D structure of the inner membrane component has been modeled by comparative molecular modeling [5,6]. From their structure analysis, it has been assessed that this RND component exists as asymmetric homotrimer [12] whose individual monomers adopt, in a concerted fashion, one of three conformations that represent different steps of the drug export process: access, binding, and extrusion (also known as loose, tight, and open, respectively) [13]. In addition, the *mexY* gene is frequently subject to mutation leading to polymorphic MexY structure that is often associated to an increased antibiotic resistance [14]. In our previous works [5,6,11], we reconstructed the EP full structure in membrane considering the aminoacidic sequences for this protein in laboratory *P. aeruginosa* strains PA01, PA7 and PA14 and used them to carry out High throughput Virtual screening (HTVS) combined with *in vitro* testing to identify powerful allosteric inhibitors of this Efflux system (EPIs). Among the identified compounds, the natural alkaloid berberine was the one which shows a good inhibitory activity when used in synergy with tobramycin associated to a low toxicity [11]. Thus, starting from this lead compound, we proceeded to modify its structure introducing an aromatic functionalization in 13-C-position and thus evaluated its activity [6]. Besides, we also go ahead in evaluating the influence of the MexY polymorphism on the berberine derivatives inhibition efficacy. For this aim, mexY gene from some clinical resistant strains were sequenced and the full 3D models of MexY proteins were totally reconstructed and compared. The *in vitro* antimicrobial and antibiofilm activity of these derivatives respect to those of berberine was also evaluated against the tobramycin resistant *P. aeruginosa* clinical strains.

Besides, biofilm (BF) production increase resistance to antibiotics [15] by avoiding the entry of drugs through the polysaccharide matrix, reducing cell growth rate and increasing efflux pumps expression [16,17]. The role of efflux pumps in biofilm formation has been hypothesized in different pathogens [16,18] and then alteration in efflux activity could affect biofilm production and enhance antibiotic susceptibility. Thus, we also proceeded to evaluate *in vitro* the berberine derivatives influence on BF production for the selected clinical strains.

.Results and Discussion

Due to the promising results obtained, [5-6] in this work we went further extending the aromatic moiety functionalization, with the final aim to enhance the affinity and subsequently the inhibitory effect, targeting an allosteric site (ALP) already identified as promising in our previous works (Scheme 1). We also included in our testing, the 13-2-methylbenzylberberine derivative (o-CH3-BERD) which previously showed an increased potency from the *in silico/in vitro* analysis towards selected *P.aeruginosa* strains [6]

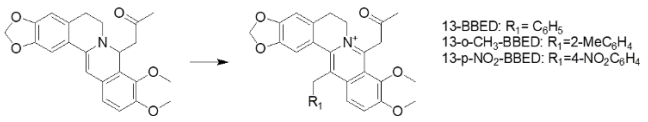

Scheme 1 Reagents and conditions: R_1Br, NaI, CH_3CN, reflux

PCR Data Analysis: MexY Sequences and alignment in clinical strains

The MexY aminoacidic sequences of all clinical strains were identified and then aligned with the *P. aeruginosa* PA7 one which represent our laboratory reference resistant strain. The alignment comparison between PA7 and the standard laboratory reference strains *P. aeruginosa* PAO1 and PA14 was already reported in our previous work [6].

As we can observe from the alignment results, all MexY proteins from clinical strains are highly conserved with some punctual mutations spread all over the aminoacidic sequences with respect to PA7 MexY (Figure SM1), but only some of them are significant in terms of changes in amino acid properties, i.e. A144S, G149D, G199D, G502D, T516A, Q525R, K526N, Q633R, G776S, Q840E. More in details, the CF30 and CF15 strains have identical primary sequences. Besides, in the CF48 strain, positions 286 and 289 correspond to two prolines instead of two threonine (T286P, T289P). In CF86 and CF04, the protein sequences are quite identical differing only for G1002A. These types of mutations could aid in predicting differences in binding energy and ligand positioning within the macromolecule, by subsequent dynamic docking studies.

Molecular Docking of Ber and its derivatives

The polymorphic MexY protein structures were built using the SwissModel server [19] in its loose (L), tight (T) and open (O) conformations. This was made necessary to build up the homotrimer in its natural quaternary structure which involves three single proteins, each one in a different conformation [20]. For the subsequent docking studies, only the protein in its tight conformation (T) was considered. The choice of evaluating this one comes from both our previous studies about the identification of possible inhibition sites in the others two MexY conformations (loose and open) (data not reported). Indeed, no allosteric sites are found out in the L and O conformations and these results are supported from literature data which refers to co-crystallized structure of AcrB in *E. coli* with its inhibitors only present in the Tight conformation. Thus, we analyzed all the possible subdomains into the protein porter domain (PD), comparing it to the described ones in the crystallized structure of the MexB [6,11].In Figure 1, the four main subdomains PC1, PC2, PN1, PN2 which allocate the two deeply studied binding sites (i.e the access pocket (AP) and the deep binding pocket (DBP)) are depicted in different colors. For the molecular docking studies aimed to detect any putative inhibition binding site, along with the 13-(2-methylbenzyl)-berberine (o-CH3-BBED) selected on the basis of our previous reported results [6],other two berberine derivatives carrying an aromatic functionalization in the 13-ring position were synthesized, namely 13-benzylberberine (13-BBED), and 13-(4-nitrobenzyl)-berberine (p-NO2-BBED). The choice of the benzyl functionalization was made to test the influence of a hydrophilic or hydrophobic substituent, that is of major importance since the ALP site is prevalently apolar in the buried cavity but contains polar residues at its entrance.

Then, for Berberine (BER) and its three chosen derivatives a blind docking study was performed on the entire surface of MexY protein for each clinical strain. The aim was to identify any potential binding site and eventually confirm the interaction of the ligands with the previously described allosteric site (ALP i.e. Allosteric Pocket) located at the interface between the periplasmic space and the external leaflet of the 1-palmitoyl2-oleoyl-sn-glycero-3-phosphocholine (POPC) bilayer [5,6,11]. Specifically, the results revealed that both BER and its derivatives can bind to the tight conformation in ALP, even if in some clinical strains MexY, BER and 13-BBED show in addition another binding site located above the allosteric one. ALP site is depicted as light green spheres in the MexY ribbon representation (Figure 1) and its aminoacidic composition is reported in Table 1.

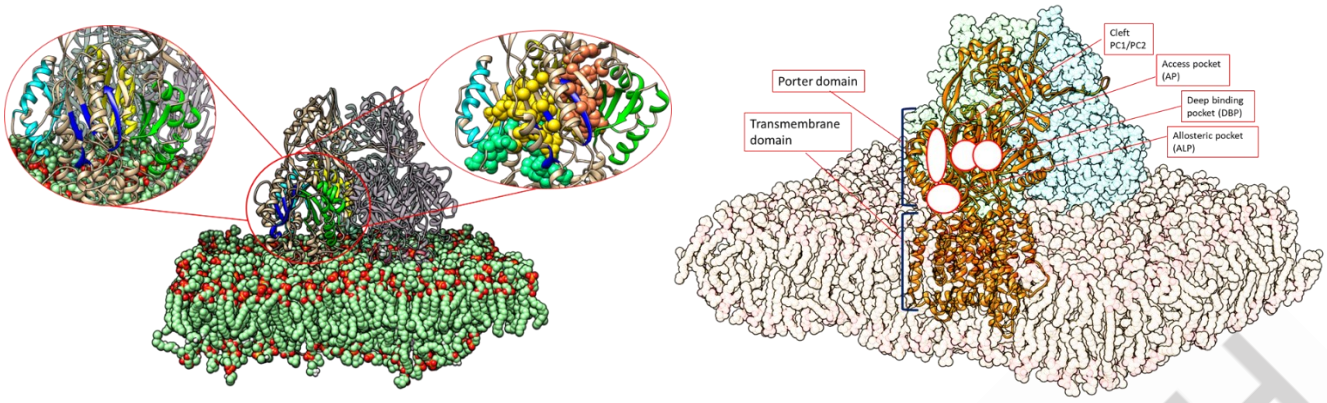

Figure 1. Left) The MexY protein homotrimer embedded within a POPC bilayer is depicted. The protein is represented using a ribbon representation, with residues that constitute subdomains colored green for the PN2 subdomain, yellow for the PN1 subdomain, blue for PC1, and cyan for PC2. PC2 is located below PC1. Another focus of the illustration shows residues of the DP in coral colour, residues of the AP in yellow, and residues of the accessory pocket in light green. Right) the MexY homotrimer with binding pockets highlighted.

Table 1. Aminoacidic composition of the Allosteric pocket (ALP), the Access pocket (AP) and within the deep binding pocket (DBP).

Access Pocket (AP)	Deep Binding Pocket (DBP)	Allosteric pocket (ALP)
K79, T90, M133, K291, S134, S619, M570, M572, M574, M661, N662, S663, L669, S671, M676, T657, M711, A713, Q840	S46, K79, S88, Y127, M133, I135, I138, S272, E273, K291, M570, M574, Y605, F623, M661, N662, S663, L669, D676	F560, L561, P562, E563, E564, S611, P665, P664, L666, S673, G674, F675, E822, Q824, Q856, S831, Q824, A825, A834, S830, E833

BER and its derivatives affinity for the MexY protein of *P. aeruginosa* PA7

Blind docking analyses were conducted on the MexY protein of the PA7 strain using Berberine and its derivatives as ligands. We identified a specific site of interaction ALP that exhibited the highest binding affinities for the ligands compared to other pockets. This peculiar cavity, referred to as the non-competitive site ALP, was previously described in our earlier works [5,6,11]. The obtained free Gibbs binding energy results -8.66 kcal/mol (calculated Ki value of 447.2 nM) for Berberine. Its derivatives displayed even higher affinities compared to the parent compound: o-CH3-BBED gained a binding energy of -10.56 kcal/mol (Ki 18.84 nM), 13-benzylberberine (13-BBED) exhibited a binding energy of -10.59 kcal/mol (Ki of 17.17 nM), and 13(4-nitrobenzyl) berberine (p-NO2-BBED) displayed a binding energy of -9.59 kcal/mol (Ki of 93.72 nM).

All the minimum energy complexes underwent molecular dynamics (MD) simulations to assess the stability of the ligands' binding in the four different homotrimer systems.

The analysis conducted at the end of the MD simulation revealed several key interactions that stabilized Berberine within the system (Figure 2). These included π-π interactions with TYR35 and PHE560, as well as π-alkyl interactions involving LEU561 and LEU669. Additionally, an H-bond was observed with Q856. The derivatives with benzylic aromatic moieties facilitated the formation of additional interactions. For instance, o-CH3-BBED and p-NO2-BBED exhibited π-alkyl interactions with ALA559 and PHE560, as well as interactions with LEU669 in the binding pocket. Many of the residues involved in these interactions were shared among the ligands, particularly those interacting with the benzo-dioxazolic group and the aromatic rings of Berberine. Other notable residues contributing to the stabilization effect included PRO665, PRO664, LEU561, MET838, LEU666, ALA825, SER673, and PHE675. Among these mentioned above, the more polar residues (i.e. SER, MET) could induce the formation of H-bonds or OH-π interactions, while the nonpolar residues were involved or in π–π (i.e. Phe) or in CH-π interactions (Figure 2).

The analysis of the calculated MM/PBSA free Gibbs binding energy indicated that all the derivatives were effective ligands for the same binding site ALP, even more so than the parent compound. For p-NO2-BBED, the aromatic moiety interacts with ALA559, while the nitro group establishes specific interactions with polar residues such as TYR829, SER830, and GLN824. This is not surprisingly since the non-competitive pocket ALP contains both nonpolar and polar residues, being the last located prevalently at its entrance.

The calculated free Gibbs binding association energies are as follows: -438.89 kJ/mol for Berberine, -503.09 kJ/mol for o-CH3-BBED, -516.04 kJ/mol for 13-BBED, and -551.477 kJ/mol for pNO2-BBED (Figure 3). Among them, the 13-(4-nitrobenzyl)-berberine exhibits the highest stability, as indicated by its lower free Gibbs binding energy. This increased stability can be attributed to the presence of different polarity of aromatic functionalization moiety.

Both molecular docking and molecular dynamics simulations consistently confirm that Berberine derivatives exhibit higher affinity compared to the parent compound. Furthermore, the

molecular specificity for the non-competitive site ALP is enhanced for these derivatives. Based on these findings, we can predict that these ligands could display similar inhibitory activity *in vitro*, but with different potency depending on the nature of their functional groups.

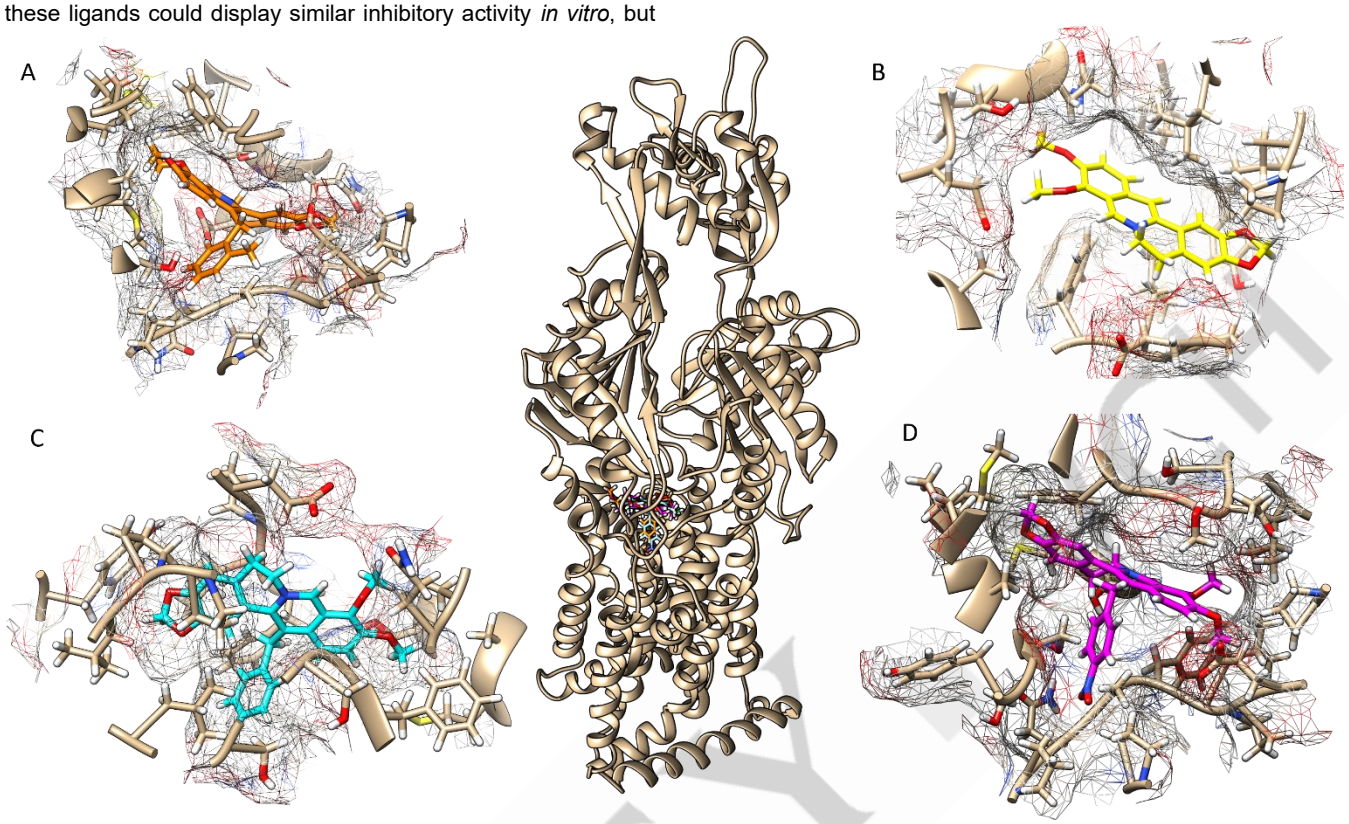

Figure 2. Interactions of all ligands [A) o-CH3-BBED (orange tubes); B) Berberine (yellow tubes); C) BBED (cyan tubes) and D) pNO2_BBED (pink tubes)] with residues within the non-competitive pocket ALP in MexY protein of PA7 strain are shown.

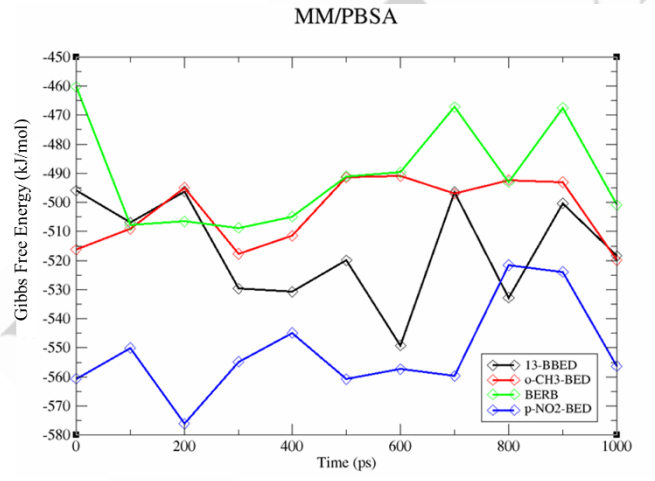

Figure 3. MM/PBSA plots for the free Gibbs binding energy of the simulated ligands-MexY^{PA07} complexes. The energy calculations were averaged for the last ns of the molecular dynamics simulations, after the system stabilization.

Ber and its derivatives affinity for MexY proteins of clinical strains.

Based on the blind docking results, Berberine occupies a different pocket in all MexY proteins of the tested clinical strains compared to that of the laboratory strain (PA7). The specific binding pocket location depends on the MexY isoform. In all clinical strains Berberine is positioned in MexY protein between the PC1 and PC2 subdomains, with varying ΔG values which are reported in detail in Table2. This binding position is quite different from the one evidenced in the same protein of the PA7 strain, and it has shown a minor affinity (-7.37/-7.54 kcal/mol vs -8.66 kcal/mol respectively). A similar trend is observed also for the 13-benzylberberine derivative which in the MexY of clinical strains is located close to the PC1 and PC2 subdomains, rather than within the previously identified allosteric site (ALP) in PA7. The affinities in this pocket are similar to Berberine as can be observed in Table2. In the MexY of PA7, this site is not occupied, and the binding occurs in the known inhibition site ALP with a binding energy of -10.59 kcal/mol. o-CH3-BBED demonstrates a preference for localization within the non-competitive site (ALP) also for MexY of clinical strains (Figure 4), even though its binding energy values differ from those found in the PA7 protein (Table 2). Both 13-4-nitrobenzylberberine and 13-2-methylbenzylberberine preferably establish interactions with the inhibition site ALP but with lower affinity. Specifically, for p-NO2-BBED the binding energies within the different MexY forms are: -7.43 kcal/mol

(Ki=3.55 μM) (CF04), -8.24 kcal/mol (Ki=906.84 nM) (CF15-CF30), -8.31 kcal/mol and Ki=811.44 nM (CF86), and -8.00 kcal/mol and Ki=1.37 μM (CF48) compared to -9.59 kcal/mol in PA7 (Table 2).

Table 2. Free Gibbs binding Energy and inhibition constant Ki for Berberine and its three derivatives in complex with MexY in PA7 and in the selected *P. aeruginosa* strains.

Strain	Berberine	13-BBED	o-CH3-BBED	p-NO2-BBED
MexY-PA7	-8.66 kcal/mol [a] Ki= 447.2 nM	-10.59 kcal/mol [a] Ki= 17.17 nM	-10.56 kcal/mol [a] Ki= 18.84 nM)	-9.59 kcal/mol [a] Ki = 93.72 nM
MexY-CF48	-7.37 kcal/mol [b] Ki=3.94 μM	-8.19 kcal/mol [b] Ki=991.94 nM	-8.36 kcal/mol [a] Ki= 746.71 nM	-8.00 kcal/mol [a] Ki= 1.37 μM
MexY-CF04	-7.53 kcal/mol [b] Ki=3.04 μM	-7.84 kcal/mol [b] Ki= 1.79 μM	-8.52 kcal/mol [a] Ki= 568.5 nM	-7.43 kcal/mol [a] Ki= 3.55 μM
MexY-CF15	-7.54 kcal/mol [b] Ki=2.97 μM	-7.69 kcal/mol [b] Ki= 2.31	-7.77 kcal/mol [a] Ki= 2.02 μM	-8.24 kcal/mol [a] Ki= 906.84 nM
MexY-CF30	-7.53 kcal/mol [b] Ki=3.02 μM	-7.69 kcal/mol [b] Ki= 2.31μM	-8.01 kcal/mol [a] Ki= 1.36 μM	-8.24 kcal/mol [a] Ki= 906.84 nM
MexY-CF86	-7.53 kcal/mol [b] Ki=3.0 μM	-8.31 kcal/mol [b] Ki= 894.7 nM	-8.19 kcal/mol [a] Ki= 986.15 nM	-8.31 kcal/mol [a] Ki= 811.44 nM

[a] ALP site. [b] PC1/PC2 site.

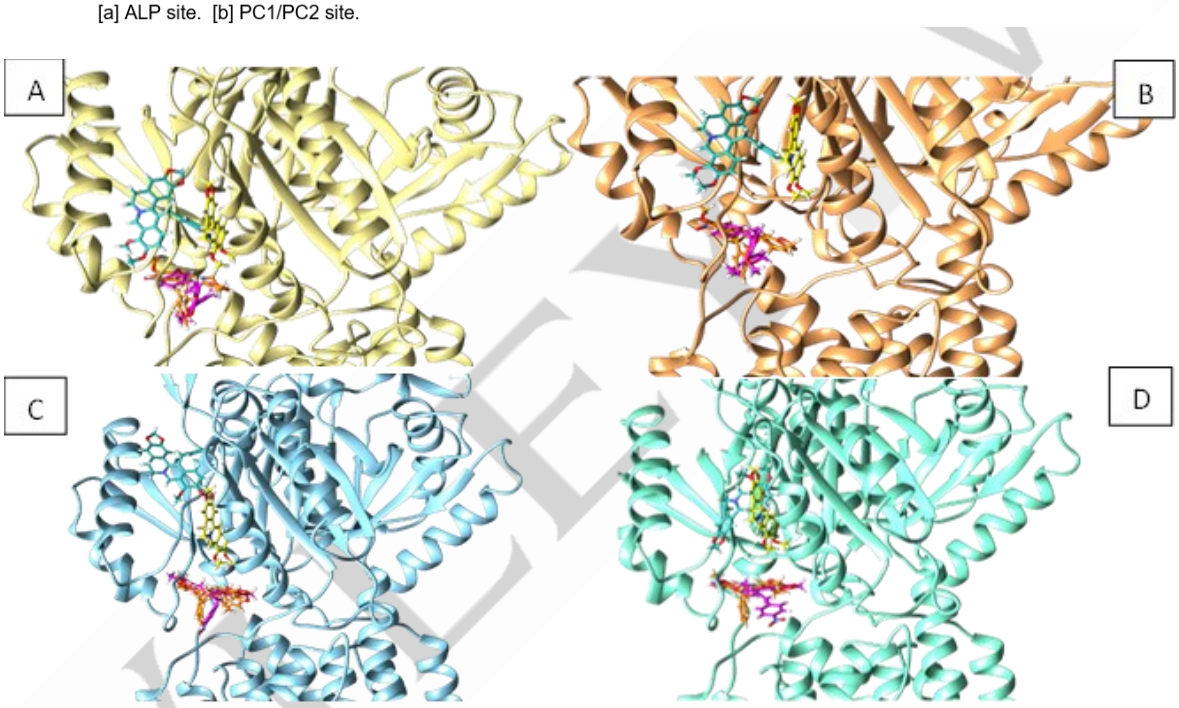

Figure 4. Docking poses of Berberine (yellow), 13(2-methylbenzyl)berberine (orange), 13-benzylberberine (cyan) and 13(4-nitrobenzyl)berberine (violet) within the MexY protein of the four clinical strains: A)CF48 (light yellow) B) CF86 (sandy brown) C) CF15-CF30 (light blue) D) CF04 (light green).

Microbiological Results

Susceptibility and Synergy tests

Susceptibility of clinical *P. aeruginosa strains* (CF48, CF15, CF30, CF04, and CF86) to tobramycin and to the three berberine derivatives (o-CH3-BBED p-BZ-BBED and p-NO2-BBED) was assessed by minimum inhibitory concentration (MIC) determination. As previously observed [6], berberine compounds (in the range 10-320 μg/ml) and 1.6% DMSO (used as solvent) showed no antimicrobial activity. Against tobramycin, all strains except for CF04 (MIC= 8 μg/ml) were resistant exhibiting MIC values ranging from 16 to 512 μg/ml (Table 3). The resistance level to aminoglycosides was potentially correlated to the presence of different resistance genes encoding antibiotic modifying-enzymes, besides to the activity of MexXY efflux pump. All strains, except one (*P. aeruginosa* CF48), carried at least one of the resistance genes detected. The gene *aph (3")-Ib* was found only in PA7, the *ant(2")-Ia* in the CF04 and CF86 strains, whereas CF15 and CF30 carried *aac(6')-Ib* and *aph(3)-IIb*. The CF86 strain was positive also for *aac(6')-Ib* and *aph(3)-IIb*.

In the checkerboard assays, only the o-CH3-BBED, compared to p-BZ-BBED and p-NO2-BBED was able to reduce tobramycin MIC in all tested strains. The o-CH3-BBED showed synergy in association with tobramycin at just 40 μg/ml causing from 2- to

16-fold decrease of tobramycin MIC (Figure 5). In particular the CF04, CF30 and CF48 strains in presence of 40 µg/ml o-CH3-BBED were fully susceptible to tobramycin (MIC≤ 4 µg/ml) (Figure 5). Furthermore, berberine derivatives were tested in association with tobramycin against the *ΔmexXY* strain *P. aeruginosa* K1525 and against the same strain complemented with the plasmid pYM004 carrying *mexXY* gene. While the deleted strain did not show any modification of its tobramycin MIC (0.25 µg/ml) in absence/presence of the three EPI compounds, the complemented strain (MIC=1 µg/ml) exhibited an 8- , 4- and 2-fold decrease in tobramycin's MIC (0.125-0.25-0.5 µg/ml) in presence of o-CH3-BBED, p-BZ-BBED and p-NO2-BBED respectively. This finding clearly highlighted the specific activity of Berberine derivatives against the MexXY-OprM pump.

Table 3 Tobramycin MIC results and aminoglycoside-resistance genes in *P. aeruginosa* clinical strains.

Strains	MIC Tobramycin (µg/ml)	*aac(6')-Ib* [a]	*aph(3'')-Ib* [a]	*aph(3)-IIb* [a]	*ant (2'')-Ia* [a]
PA7	256	-	+	-	-
CF48	32	-	-	-	-
CF04	8	-	-	-	+
CF15	16	+	-	+	-
CF30	16	+	-	+	-
CF86	512	+	-	+	+

[a] Resistance genes

Biofilm production and antibiofilm activity of o-CH3-berberine derivatives

All the strains were first tested for their biofilm production in LB broth as previously described in literature [21]. The reference PA7 and CF30 strains were categorized as Strong Biofilm Producers (SBP), CF86 and CF04 strains were Moderate Biofilm Producers (MBP) whereas CF48 and CF15 strains were weak biofilm producers (WBP). Then biofilm formation by SBP and MBP strains was performed in presence of tobramycin to assess the antibiofilm activity of antibiotic. Overall, growth in biofilm of strains was affected by the presence of tobramycin at 1x and 2xMIC values with a significant reduction of biofilm production even if most strains remained in the same starting category (Table 4, Figure 6).

Given the involvement of efflux pumps in biofilm formation [16], the influence of o-CH3-BBED alone and in association with tobramycin was also assessed for SBP and MBP strains.

o-CH3-BBED used alone at 40 µg/ml concentration, caused a greater reduction of biofilm production respect to tobramycin (1XMIC).

To investigate if a low concentration of tobramycin was able to reduce biofilm formation in presence of the EPI, we used tobramycin at concentration of ½XMIC in association with o-CH3-BBED at 40 and 80 µg/ml concentration (Figure 6). As predicted in LB supplemented with ½ XMIC of tobramycin and 40 µg/ml of o-CH3-BBED a significant reduction of biofilm production was observed in all the strains compared to the production in LB broth. The reduction was significant in *P. aeruginosa* CF86 and CF04 also when compared to the production in presence of tobramycin alone (at MIC and 2XMIC). However, in the CF30 e CF86 strains biofilm production in broth with tobramycin (½XMIC) and EPI was higher. The antibiofilm activity was not always improved using 80 µg/ml of EPI in combination with tobramycin (Figure 6).

Therefore, the antibiofilm activity of o-CH3-BBED in association with tobramycin seems to be strain-dependent; further analysis are required to confirm its ability to interfere with biofilm production.

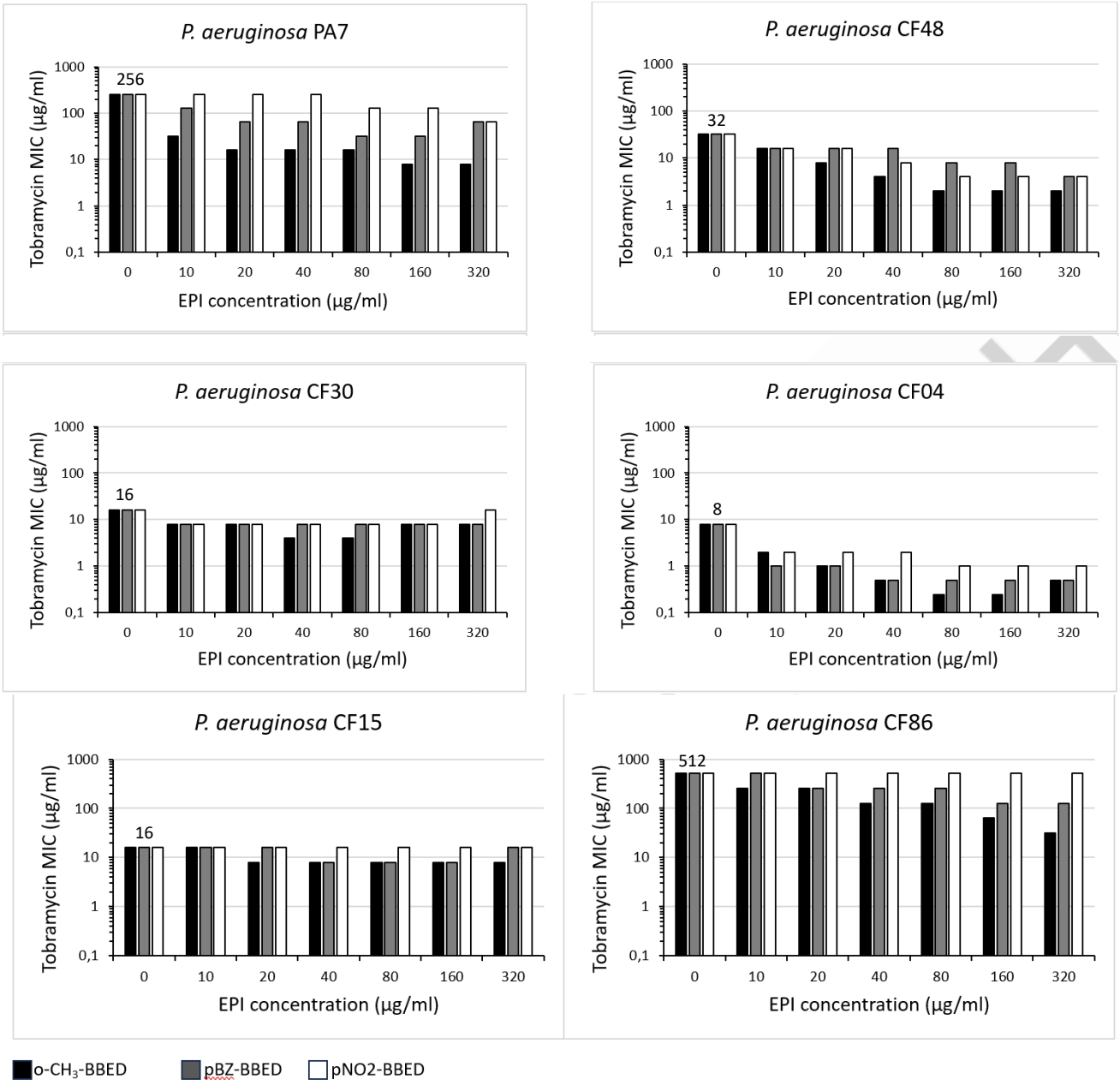

Figure 5. Results from checkerboard assays. Reduction of tobramycin MIC in presence of increasing concentration of the three Berberine-derivatives. The numbers reported above the bars are the Tobramycin MIC values of each strain in absence of EPI compounds.

Table 4. Antibiofilm activity of different concentration of tobramycin alone and in combination with o-CH3-BBED

P. aeruginosa strain	Biofilm producer in LB			Biofilm producer in LB with tobramycin (µg/ml) at MIC			Biofilm producer in LB with tobramycin (µg/ml) at 2XMIC			Biofilm producer in LB with1/2MIC of tobramycin and 40 µg/ml o-CH_3-BBED			Biofilm producer in LB with1/2MIC of tobramycin and 80 µg/ml o-CH_3-BBED			Biofilm producer in LB with 40 µg/ml o-CH_3-BBED			Biofilm producer in LB with 80 µg/ml o-CH_3-BBED		
PA7	A	3,9	Strong	A	1,1	Moderate	A	0,4	NP	A	0,8	Moderate	A	0,6	Moderate	A	1	Moderate	A	1,5	Moderate
	SD	0,7		SD	0,5		SD	0,02		SD	0,1		SD	0,02		SD	0,1		SD	0,4	
	ODc	0,5		ODc	0,3		ODc	0,3		ODc	0,3		ODc	0,3		ODc	0,4		ODc	0,4	
CF30	A	3,9	Strong	A	2,2	Strong	A	2,1	Strong	A	2,4	Strong	A	2,5	Strong	A	1,5	Strong	A	2,2	Strong
	SD	0,5		SD	0,3		SD	0,04		SD	0,1		SD	0,3		SD	0,4		SD	0,3	
	ODc	0,5		ODc	0,5		ODc	0,3		ODc	0,3		ODc	0,3		ODc	0,3		ODc	0,3	
CF48	A	2,3	Weak	A	0,3	Weak	A	0,25	NP	A	-	ND	A	-	ND	A	-	ND	A	-	ND
	SD	0,2		SD	0,003		SD	0,005		SD	-		SD	-		SD	-		SD	-	
	ODc	0,5		ODc	0,3		ODc	0,3		ODc	-		ODc	-		ODc	-		ODc	-	
CF86	A	1,5	Moderate	A	0,8	Moderate	A	0,8	Moderate	A	1,1	Moderate	A	1,8	Strong	A	1	Moderate	A	1,2	Strong
	SD	0,2		SD	0,2		SD	0,2		SD	0,1		SD	0,2		SD	0,09		SD	0,1	
	ODc	0,4		ODc	0,3		ODc	0,3		ODc	0,3		ODc	0,3		ODc	0,36		ODc	0,3	
CF04	A	2,8	Moderate	A	1,0	Moderate	A	0,9	Moderate	A	0,5	Weak	A	0,3	Weak	A	0,7	Weak	A	0,7	Moderate
	SD	0,1		SD	0,04		SD	0,005		SD	0,03		SD	0,03		SD	0,04		SD	0,02	
	ODc	1,4		ODc	0,3		ODc	0,3		ODc	0,3		ODc	0,3		ODc	0,8		ODc	0,3	
CF15	A	0,8	Weak	A	0,5	Weak	A	0,2	NP	A	-	ND	A	-	ND	A	-	ND	A	-	ND
	SD	0,4		SD	0,01		SD	0,03		SD	-		SD	-		SD	-		SD	-	
	ODc	0,5		ODc	0,3		ODc	0,3		ODc	-		ODc	-		ODc	-		ODc	-	

A: Average; SD: Standard Deviation; ODc: Optical Density cut-off; NP: Not Producer; ND: Not Determined

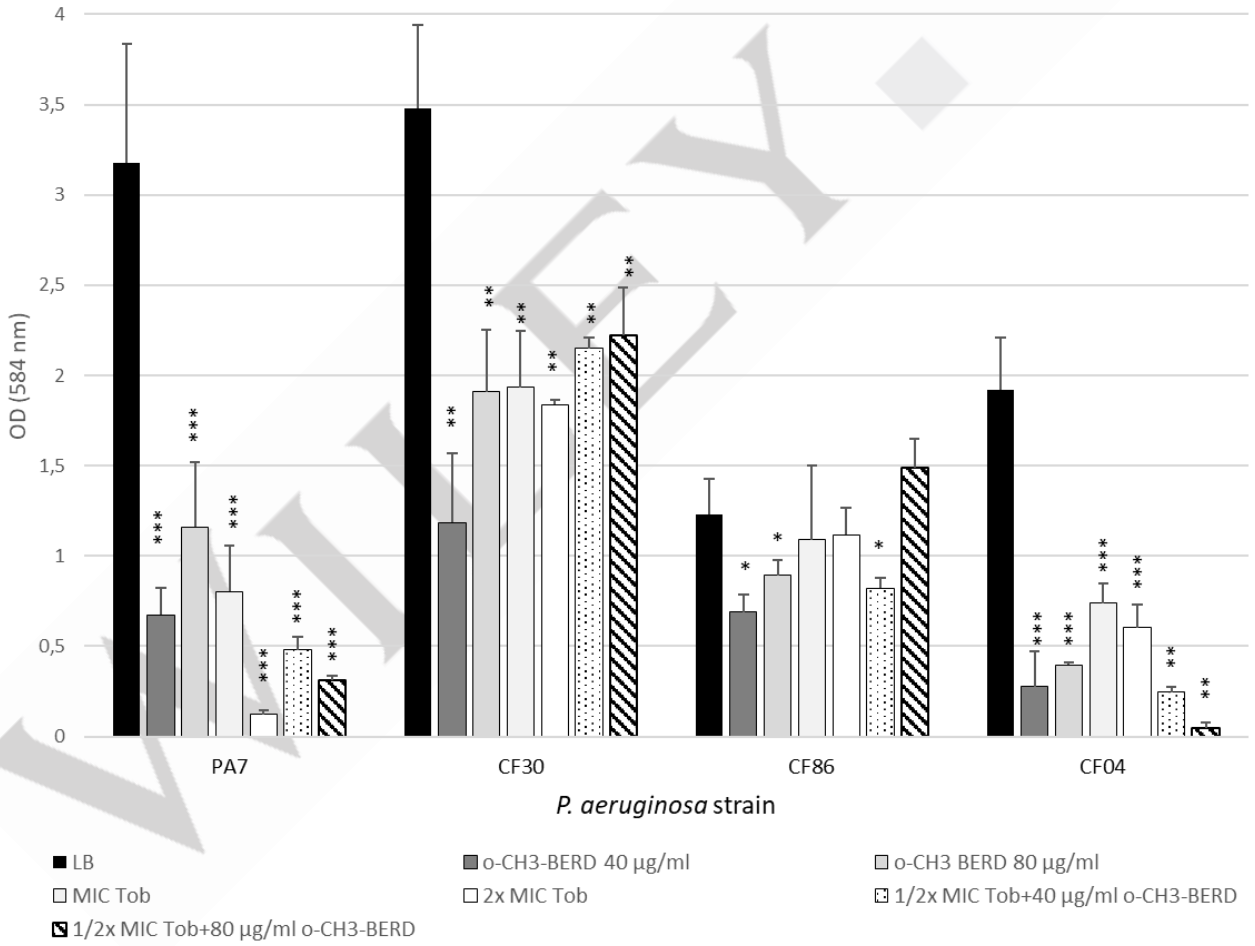

Figure 6. OD quantification of biofilm production in *Pseudomonas aeruginosa* strains grown in: LB broth, in LB with o-CH3-BBED (40 µg/ml or 80 µg/ml), in LB with tobramycin (Tob) (MIC, 2XMIC), in LB with a combination of tobramycin (½ X MIC) and o-CH3-BBED (40 µg/ml or 80 µg/ml). The results are reported as the average of three biological replicates ± standard deviation. The significance of the reduction of biofilm production was assessed in comparison to biofilm production in LB broth and it has been indicated as follow: *= $p < 0,05$; **= $p < 0,001$; ***= $p \leq 0,0001$.

Overall, considering all the results obtained we can point out the following aspects:
(1) The positioning of the ligands within each protein is clearly influenced by both the chemical functionalization of the Berberine skeleton and the aminoacidic composition of the MexY protein. The chemical aromatic substituents generally enhance the binding affinity within the protein pockets, particularly in the non-competitive site ALP. From the molecular docking and dynamics results, in PA7, all the three considered derivatives, the 13-(3-methylbenzyl)-berberine, 13-benzyl-berberine and 13-(4-nitrobenzyl)-berberine exhibited higher scores compared to Berberine.
(2) Besides in all the MexY protein variants, all the berberine derivatives except for the 13-BBED binds preferably in ALP, with different binding energy values which depends on both the MexY and ligands' structures. On the contrary, Berberine and the 13-benzylberberine (13-BBED) are positioned in a binding pocket located between the subdomains PC1 and PC2, in an upper region with respect to ALP. This difference can be ascribed mainly to the amino acid variations within these proteins compared to the MexY protein of the laboratory strain PA7. These findings highlight the importance of considering possible mutations within target proteins.
(3) Overall, the microbiological results confirm the *in silico* findings. A peculiar behavior is observed for the 13-(4-nitrobenzyl)-berberine. In fact, this compound showed a computed higher affinity according to the free Gibbs binding energy values obtained after the MD simulation, but it showed a reduced *in vitro* activity, even if increasing with its concentration (only exception CF15 and CF86). This behavior can be explained considering the increased local polarity of the functional group in the aromatic moiety which could affect the derivative capability to penetrate the external bacterial membrane, thus preventing it to reach the ALP binding pocket, which is located deep inside the periplasmic environment. Studies are ongoing to explore the potential of these berberine derivatives within liposomal nano vectors, with the aim of enhancing its cell membrane permeability and support this suggestion.

Experimental Methods

General Synthesis Information

The materials and reagents used in the synthetic procedures were purchased from Sigma Aldrich Co. (Stenheim, Germany) and used without purification. Dihydroberberine was synthesized by the reduction of berberine according to the reported procedure [22]. All solvents were analytically pure and dried before use. TLC were carried out on aluminum sheets precoated with silica gel 60 F254 (Merck). Column chromatography was performed using silica gel 60 (230–400 mesh).
High-resolution MS (HRMS) ESI analyses were performed on a Xevo G2-XSQTof (Waters) mass spectrometer. Mass spectrometric detection was performed in the in the positive ion mode. The 1H and 13C NMR spectra were recorded at 500 and 125 MHz, respectively, on a Bruker Ascend 500 Avance III HD spectrometer. Chemical shifts (δ) are reported in ppm relative to TMS and coupling constants (J) in Hz. Melting points were obtained on an Electrothermal apparatus IA 9000 and are uncorrected.

General Synthesis Procedure of Berberine Derivatives

The 13-BBED and o-CH3-BBED and the new Berberine derivatives pNO2-BBED and have been synthesized (Scheme 1) according to previous work [6] following the Kotani at al. protocol [23] with minor changes. Thus, after dropwise addition of the appropriate benzyl bromide (1.0 mmol) to a dihydroberberine (1 equiv) and KI (2 equiv) CH_3CN (40 mL) solution, the reaction mixture was refluxed under stirring for 4 h. After filtration and solvent evaporation, the crude residue was purified by silica gel column chromatography using CHCl3/CH3OH (50:1) as eluent. The characterization data of the compounds and 13-BBED o-CH3-BBED obtained were identical to those given in the literature [24]

*13-(4-nitrobenzyl) berberine (**p-NO2-BBED**)*
Brown Solid; yeld: 72%; 1H NMR (CDCl3 ,500MHz): δ 3.27-3.32 (m, 2H), 4.01 (s, 3H), 4.34 (s, 3H), 4.84 (s, 2H), 5.09-5.15 (m, 2H), 6.00 (s, 2H), 6.78 (s, 1H), 6.88 (s, 1H), 7.53 (d, J=7.9 Hz, 1H), 7.73 (d, J=9.2 Hz, 1H), 8.19 (d, J=9.2 Hz, 2H), 10.30 (s, 1H); 13C NMR (125 MHz, CDCl3): δ 28.3, 36.6, 56.9, 58.1, 63.0, 102.1, 108.5, 108.7, 119.7, 120.6, 121.8, 124.5, 126.0, 128.7, 129.1, 133.2, 133.6, 137.9, 145.8, 146.1, 146.6, 147.0, 147.3, 150.2, 150.5; Calcd. neutral mass for C27H23N2O6: 471.1556 Da; HRMS: m/z = 471.1554 (M+)
*13-benzylberberine (**13-BBED**)*
1H NMR (CDCl3 ,500MHz): δ 3.27-3.32 (m, 2H), 4.01 (s, 3H), 4.39 (s, 3H), 4.68 (s, 2H), 5.14-5.23 (m, 2H), 5.99 (s, 2H), 6.87 (s, 1H), 6.95 (s, 1H), 7.12 (d, J=7.3 Hz, 1H), 7.28-7.32 (m, 1H), 7.34-7.38 (m, 2H), 7.62 (d, J=9.5 Hz, 1 H), 7.70 (d, J=9.5 Hz, 1 H), 10.40 (s, 1H); 13C NMR (125 MHz, CDCl3): δ 28.4, 36.6, 56.9, 58.1, 63.2, 101.9, 108.5, 108.8, 120.0, 120.9, 121.7, 125.7, 127.2, 127.9, 129.4, 130.2, 133.4, 133.8, 137.5, 138.1, 146.0, 146.3, 147.1, 150.0, 150.4. Calcd. neutral mass for C27H24NO4: 426.1700Da; HRMS: m/z = 426.1698 (M+)
*13-(2-methylbenzyl) berberine (**o-CH3-BBED**)*
1H NMR (CDCl3 ,500MHz): δ 2.47 (s, 3H), 3.30-3.34 (m, 2H), 4.03 (s, 3H), 4.44 (s, 3H), 5.18-5.26 (m, 2H), 6.00 (s, 2H), 6.65 (d, J=7.6 Hz, 1H), 6.84 (s, 1H), 6.88 (s, 1H), 7.06-7.10 (m, 1H), 7.23-7.27 (m, 1H), 7.37 (d, J=7.6 Hz, 1H), 7.53 (d, J=9.5 Hz, 1H), 7,69 (d, J=9.5 Hz, 1H), 10.47 (s, 1H). Calcd. neutral mass for C28H26NO4: 440.1856 Da; HRMS: m/z = 440.1848 (M+)

Microbiological methods

Bacterial strains

In this study the *P. aeruginosa* laboratory strains PA7, K1525 (and its derivative containing the plasmid pYM004) previously described [6] and five clinical *P. aeruginosa* strains were used. Clinical strains, belonging to a previous collection [11], were isolated from sputum samples of patients with fibrosis cystic and were anonymously provided by the analysis laboratory of the Marche region Hospital.

Susceptibility assays.

Susceptibility to tobramycin and berberine derivatives was assessed by broth microdilution method according to CLSI guidelines for MIC determination (ref CLSI). Two-fold serial dilution of tobramycin (from 256 µg/ml to 0.25 µg/ml) and berberine derivatives (from 320 µg/ml to 10 µg/ml) were prepared in Mueller Hinton II broth (MHII, Oxoid). Dimethyl sulfoxide (DMSO, Sigma) was used as solvent for Berberine and its derivatives; the final concentration of DMSO in the microtiter wells was 1.6%. Tobramycin MIC was determined both in presence and absence of the same final % of DMSO to exclude a DMSO interfering on MIC results. Synergy between berberine (or berberine derivatives) and tobramycin was evaluated by checkerboard assays performed as previously described [6].

Amynoglicoside resistance genes

The detection of some resistance genes [*aac(6')-Ib*; *ant(2")-Ia*; *aph(3")-Ib*; *aph(3)-IIb*] encoding aminoglycoside-modifying enzymes, frequently found in *P. aeruginosa* was performed using primers and PCR protocols described elsewhere [3]. For the amplification of *aph(3)-IIb* gene new primer pair (FW 5'-TTGCCCGCAGGTGCTGAACG and REV 5'-CAGCAGATTTGGCAGGCAGGC) was designed in this study.

Antibiofilm activity

Experiments for biofilm production have been performed in LB broth in microtiter plates. Crystal violet staining of biofilm, followed by its quantification by spectrophotometry (at 584 nm) has been performed as previously described by Stepanovic *et al.* with some modification [21]. The data were interpreted according to the Optical Densities (OD) of the bacterial films after staining. Hence according to their ability to produce biofilm they are distinguished into four categories of Biofilm Producers (BP): strong, moderate, weak or non-producer. Cut-off OD (OD_c) was defined as 3 times the standard deviation of the mean OD of the blank. Strains were classified as follow:

$OD \leq OD_C$ Non-Biofilm Producer (NBP)

$OD_C < OD \leq 2OD_C$ Weak Biofilm Producer (WBP)

$2\ OD_C < OD \leq 4OD_C$ Moderate Biofilm Producer (MBP)

$OD > 4OD_C$ Strong Biofilm Producer (SBP)

The effect of tobramycin and o-CH3-BBED on the biofilm formation by *P. aeruginosa* strains was evaluated.

Biofilm production was first evaluated in LB broth containing tobramycin (at MIC and 2X MIC concentrations) or o-CH3-BBED (at 40 µg/ml or 80 µg/ml) alone. Then biofilm production was assessed in presence of their combinations: tobramycin at ½ XMIC with o-CH3-BBED at 40 µg/ml or 80 µg/ml. Results were reported as the average of three replicates ± standard deviation.

Statistical Analysis. The significance of the change in biofilm production in LB supplemented with tobramycin (or o-CH3-BBED, or tobramycin and o-CH3-BBED) and in LB broth was assessed by the Student's t test. Statistical significance was defined by a p-value lower than 0.05 ($p < 0.05$).

Computational methods

MexY Sequences alignment. The *mexY* gene main variable regions were identified comparing the gene sequence of *P. aeruginosa* PA7 (NC_009656.1) to a number of strain specific sequences. Two amplicons of these regions (respectively of 270 and 588 bp) were obtained by PCR using the primer pairs mexY-F 5′ -TGGAAGTGCAGAACCGCCTG-3′ /mexY-R 5′ -AGGTCAGCTTGGCCGGGTC-3′ [25] and YF 5′ -CGTGAGCATGGACGAGATCA-3′ /YR 5′ -ATGATGGTGATCAGGCCGAC-3′ [11]. The amplicons were purified using Gene Elute PCR Cleanup kit (Sigma-Aldrich SRL) and directly sequenced using BigDye Terminator v.1.1 Cycle Sequencing kit according to the manufacturer's instructions. Sequences were analyzed on an ABI Prism 310 Genetic Analyzer (Applied Biosystems, Foster City, CA, USA). The consensus sequences thus obtained were compared to the PAO1 sequence. The MAFFT algorithm was used to align the protein sequences analyzed with the corresponding MexY regions of *P. aeruginosa* PA7. The MAFFT sequence alignment has been done setting the BLOSUM62 matrix and 1.52 gap penalty. Protein sequences from the nucleotide conversion were obtained, the correct open reading frame has been chosen for obtaining the right protein translation. Conversion of the nucleotide sequences to the corresponding amino acid sequences (one for each *P. aeruginosa* strain tested) was performed with Expasy translate tool (https://web.expasy.org/translate/). The multi-alignment obtained was displayed with Espript3 tool [26].

Protein 3D Modeling from sequence analysis. The optimized 3D structure of the MexY trimer of PA7 strain developed as previously described [5] was used as a template to visualize the mutated amino acid positions with respect to the putative berberine binding sites. Any differences in protein surface and 3D structure were investigated using Chimera software [27,28]. Three-dimensional structures of the MexY proteins were modeled as described previously using MexB (pdb code 2V50) as template [11], and employed to investigate the binding modes of berberine. The 3D MexY structures were minimized using CHARMM36m force field [29] as implemented in the GROMACS 2020.6 software package [30,31]. A robust energy minimization protocol consisting of 10 000 cycles with the steepest descent minimization algorithm was then applied, followed by 5000 cycles using the conjugate gradient algorithm until the threshold (Fmax < 100 kJ mol^{-1}) was reached.

Molecular Docking. Starting from the minimized MexY structures, a molecular docking procedure was used to investigate the binding modes of berberine to the five tobramycin extrusion protein variants. Automated molecular docking of the berberine−MexY complexes of different *P. aeruginosa* strains was performed with MGLTools/Autodock 4.2.6 [32]. A blind docking approach was used to identify the putative binding sites for all MexY polymorphic forms as already reported in our recent work on PA01 [11] then focused docking procedures were used for each MexY model, and the Lamarckian genetic algorithm (GA) was applied to handle ligand−protein interactions. A grid map centered in the ligand and extending around the cleft, with points spaced equally at 0.525$Å^3$ and 0.375 $Å^3$ intervals (for blind docking and

focused docking respectively), was generated to estimate the binding docking energy. The docking parameters were set to default values except for the number of GA runs (100), the energy evaluations (25 000 000), the maximum number of top individuals that automatically survive (0.1), and the step size for translation (0.2 Å). The final docked ligands−MexY complexes were ranked according to the predicted binding energy and arranged into clusters according to root-mean-square deviation (RMSD) values. The cluster of each complex (containing 90% of the docked structures found by the procedure) characterized by the lowest energy was then used for refinement using an assessed protocol [33,34].

Molecular Dynamics of the MexY−Ligand Complexes in Membranes. Molecular dynamics simulations were performed using GROMACS (version 2020.6) [30]. The MexY-inhibitor models have been oriented in the membrane through the OPM (Orientation of Proteins in Membrane) server (http://opm.phar.umich.edu/server.php), which generates the coordinates along the Z axis, and we used CHARMM GUI (www.charmm-gui.org) to build a membrane composed of 800 1-palmitoyl2-oleoyl-sn-glycero-3-phosphocholine (POPC) molecules. Using these coordinates, we obtained a MexY-trimer (with docked ligands) system properly surrounded by the lipid matrix that has been appropriately solvated with water (about 10 000) and ions (to reach 0.15 M NaCl, adding Na^+ and Cl^- ions also to balance the trimer charge). We used CHARMM36m force field parameters [29] for the protein and lipids and the TIP3P [35] model for solvent as implemented in GROMACS 2020.6. Six equilibration phases in thermodynamic ensembles NVT and NPT were conducted. The production phase consisted of 30-50 ns of NPT simulation setting the pressure parameters at 1atm using Parrinello-Rhaman barostat [36,37].

The MD production phase length has been tuned from RMSD graphs considering the ligand− protein complexes steady state (average deviation ΔRMSD < 0.100 ± 0.05). The timestep used was 0.002 ps, and coordinates were written out every 10 ps, while energy data were collected every 2 ps. The temperature was set to 300 K using the V-rescale thermostat. Periodic boundary conditions (PBCs) were applied in all directions using a neighbor searching algorithm setting at 1.0 nm the cutoff distance for the shortrange neighbor list. Smooth particle mesh Edward (PME) algorithm was used to estimate the electrostatic interactions [38]. The cut-off range of electrostatic and Van-der-Waals interactions was set to 1.6 Å. The free Gibbs binding energy was calculated with the MM-PBSA method (molecular mechanics/Poisson−Boltzmann surface area) using the g_mmpbsa tool [39] considering the last 1 ns after stabilization with default settings [40,41]. During the production run, snapshots were extracted every 10 ps, and energetic terms were calculated. The root mean square error (RMSD) was evaluated along all the MD trajectories frames with GROMACS tools. Results are in terms of average and standard deviations for all energetic components.

Conclusion

In conclusion, we pointed out that the aminoacidic composition of MexY in different strains of the same bacterial species is useful for predicting potential ligand positioning. This is important since different occupied binding pockets could affect the ligand's affinity and the associated *in vitro* activity. Moreover, the different activity of berberine derivatives in association with tobramycin was strain-dependent and could be related not only to the isoforms of MexY but also to multiple resistance mechanisms to aminoglycoside displayed by each strain. In strains carrying various genes encoding aminoglycoside modifying-enzymes, the effect of EPI was less evident on tobramycin susceptibility since resistance phenotype was only partially affected by the activity of efflux pumps. Conversely the antibiofilm effect of these new EPIs is promising and should further investigated considering that the reduction of biofilm production could improve penetration and activity of antibiotics into bacterial cells.

Acknowledgements

The author R.G. acknowledges financial support from the European Union—Next Generation EU (project code: ECS00000041; project title: Innovation, digitalization and sustainability for the diffused economy in Central Italy—VITALITY).

Keywords: Efflux Pump inhibitors • *Pseudomonas Aeruginosa* • Berberine • Molecular docking • Antibiotic synergism

[1] A. Zahedi Bialvaei, M. Rahbar, R. Hamidi-Farahani, A. Asgari, A. Esmailkhani, Y. Mardani Dashti, S. Soleiman-Meigooni, Microbial Pathogenesis 2021, 153, 104789.

[2] K. Jeannot, M. L. Sobel, F. El Garch, K. Poole, P. Plésiat, J Bacteriol 2005, 187, 5341–5346.

[3] A. D. Michalska, P. T. Sacha, D. Ojdana, A. Wieczorek, E. Tryniszewska, Braz. J. Microbiol. 2014, 45, 1455–1458.

[4] X. Xu, H. Yi, J. Wu, T. Kuang, J. Zhang, Q. Li, H. Du, T. Xu, G. Jiang, G. Fan, Biomedicine & Pharmacotherapy 2021, 133, 110984.

[5] E. Laudadio, N. Cedraro, G. Mangiaterra, B. Citterio, G. Mobbili, C. Minnelli, D. Bizzaro, F. Biavasco, R. Galeazzi, J. Nat. Prod. 2019, 82, 1935–1944.

[6] G. Giorgini, G. Mangiaterra, N. Cedraro, E. Laudadio, G. Sabbatini, M. Cantarini, C. Minnelli, G.Mobbili, E. Frangipani, F. Biavasco, R. Galeazzi, Molecules 2021, 26, 6644.

[7] N. Masuda, E. Sakagawa, S. Ohya, N. Gotoh, H. Tsujimoto, T. Nishino, Antimicrob Agents Chemother 2000, 44, 2242–2246.

[8] M. S. Mulani, E. E. Kamble, S. N. Kumkar, M. S. Tawre, K. R. Pardesi, Front. Microbiol. 2019, 10, 539.

[9] G. Sennhauser, M. A. Bukowska, C. Briand, M. G. Grütter, Journal of Molecular Biology 2009, 389, 134–145.

[10] S. Murakami, R. Nakashima, E. Yamashita, A. Yamaguchi, Nature 2002, 419, 587–593.

[11] G. Mangiaterra, N. Cedraro, E. Laudadio, C. Minnelli, B. Citterio, F. Andreoni, G. Mobbili, R. Galeazzi, F. Biavasco, J. Nat. Prod. 2021, 84, 993–1001.

[12] P. Ruggerone, S. Murakami, K. M. Pos, A. Vargiu, CTMC 2013, 13, 3079–3100.

[13] S. Murakami, R. Nakashima, E. Yamashita, T. Matsumoto, A. Yamaguchi, Nature 2006, 443, 173–179.

[14] S. Guénard, C. Muller, L. Monlezun, P. Benas, I. Broutin, K. Jeannot, P. Plésiat, Antimicrob Agents Chemother 2014, 58, 221–228.

[15] L. K. Vestby, T. Grønseth, R. Simm, L. L. Nesse, Antibiotics 2020, 9, 59.

[16] I. Alav, J. M. Sutton, K. M. Rahman, Journal of Antimicrobial Chemotherapy 2018, 73, 2003–2020.

[17] M. N. Hajiagha, H. S. Kafil, Infection, Genetics and Evolution 2023, 112, 105459.

[18] A. Fahmy, A. Srinivasan, M. A. Webber, in Efflux-Mediated Antimicrobial Resistance in Bacteria (Eds.: X.-Z. Li, C.A. Elkins, H.I. Zgurskaya), Springer International Publishing, Cham, 2016, pp. 651–663.

[19] A. Waterhouse, M. Bertoni, S. Bienert, G. Studer, G. Tauriello, R. Gumienny, F. T. Heer, T. A. P. de Beer, C. Rempfer, L. Bordoli, R. Lepore, T. Schwede, Nucleic Acids Research 2018, 46, W296–W303.

[20] M. A. Seeger, A. Schiefner, T. Eicher, F. Verrey, K. Diederichs, K. M. Pos, Science 2006, 313, 1295–1298.

[21] S. Stepanović, D. Vuković, I. Dakić, B. Savić, M. Švabić-Vlahović, Journal of Microbiological Methods 2000, 40, 175–179.

[22] H. Liu, L. Wang, Y. Li, J. Liu, M. An, S. Zhu, Y. Cao, Z. Jiang, M. Zhao, Z. Cai, L. Dai, T. Ni, W. Liu, S. Chen, C. Wei, C. Zang, S. Tian, J. Yang, C. Wu, D. Zhang, H. Liu, Y. Jiang, ChemMedChem 2014, 9, 207–216.

[23] K. Kotani, M. Matsumura, Y. Morita, J. Tomida, R. Kutsuna, K. Nishino, S. Yasuike, Y. Kawamura, Antibiotics 2019, 8, 212.

[24] J. Wang, T. Yang, H. Chen, Y.-N. Xu, L.-F. Yu, T. Liu, J. Tang, Z. Yi, C.-G. Yang, W. Xue, F. Yang, European Journal of Medicinal Chemistry 2017, 127, 424–433.

[25] H. Oh, J. Stenhoff, S. Jalal, B. Wretlind, Microbial Drug Resistance 2003, 9, 323–328.

[26] X. Robert, P. Gouet, Nucleic Acids Research 2014, 42, W320–W324.

[27] G. Mangiaterra, E. Laudadio, M. Cometti, G. Mobbili, C. Minnelli, L. Massaccesi, B. Citterio, F. Biavasco, R. Galeazzi, Med Chem Res 2017, 26, 414–430.

[28] E. F. Pettersen, T. D. Goddard, C. C. Huang, G. S. Couch, D. M. Greenblatt, E. C. Meng, T. E. Ferrin, J. Comput. Chem. 2004, 25, 1605–1612.

[29] J. Huang, S. Rauscher, G. Nawrocki, T. Ran, M. Feig, B. L. De Groot, H. Grubmüller, A. D. MacKerell, Nat Methods 2017, 14, 71–73.

[30] B. Hess, C. Kutzner, D. Van Der Spoel, E. Lindahl, J. Chem. Theory Comput. 2008, 4, 435–447.

[31] K. Lindorff-Larsen, S. Piana, K. Palmo, P. Maragakis, J. L. Klepeis, R. O. Dror, D. E. Shaw, Proteins 2010, 78, 1950–1958.

[32] G. M. Morris, R. Huey, W. Lindstrom, M. F. Sanner, R. K. Belew, D. S. Goodsell, A. J. Olson, J. Comput. Chem. 2009, 30, 2785–2791.

[33] R. Galeazzi, E. Laudadio, E. Falconi, L. Massaccesi, L. Ercolani, G. Mobbili, C. Minnelli, A. Scirè, L. Cianfruglia, T. Armeni, Org. Biomol. Chem. 2018, 16, 5167–5177.

[34] G. Rosita, C. Manuel, M. Franco, N. Cinzia, F. Donatella, L. Emiliano, M. Luca, G. Roberta, Mol. BioSyst. 2015, 11, 208–217.

[35] W. L. Jorgensen, C. Jenson, J. Comput. Chem. 1998, 19, 1179–1186.

[36] M. Parrinello, A. Rahman, Journal of Applied Physics 1981, 52, 7182–7190.

[37] Q. Ke, X. Gong, S. Liao, C. Duan, L. Li, Journal of Molecular Liquids 2022, 365, 120116.

[38] H. G. Petersen, The Journal of Chemical Physics 1995, 103, 3668–3679.

[39] R. Kumari, R. Kumar, Open Source Drug Discovery Consortium, A. Lynn, J. Chem. Inf. Model. 2014, 54, 1951–1962.

[40] W. M. Botello-Smith, R. Luo, J. Chem. Inf. Model. 2015, 55, 2187–2199.

[41] D. Greene, W. M. Botello-Smith, A. Follmer, L. Xiao, E. Lambros, R. Luo, J. Phys. Chem. B 2016, 120, 12293–12304.

Entry for the Table of Contents

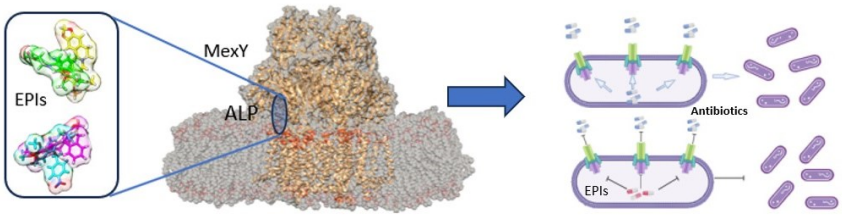

Unveiling Strategies to Combat Drug Resistance: Our study delves into the battle against drug resistance in aminoglycosides resistant *Pseudomonas aeruginosa*, focusing on the MexXY-OprM multidrug efflux pump system. We explore the design of novel efflux pump inhibitors, targeting MexY at an identified allosteric site (ALP). Lead compound Berberine and its derivatives show promise in inhibiting the pump and reducing biofilm production, offering new avenues in the fight against chronic pulmonary diseases.